Iranian Journal of Science and Technology, Transactions of Electrical Engineering
https://doi.org/10.1007/s40998-020-00402-9

RESEARCH PAPER

Proposed Application for Rate of Change of Phasor Voltage in Fault Detection and Coordination Studies in MV Distribution Networks

Mohamed Ahmed Dawoud[1] · Doaa Khalil Ibrahim[1] · Mahmoud Ibrahim Gilany[1] · Aboul'fotouh El'gharably[2]

Received: 16 June 2020 / Accepted: 7 December 2020

Abstract
Selectivity, reliability and security of electrical distribution systems are important issues in modern power systems. The protection coordination approach that depends on fault current only is no longer valid for medium voltage (MV) distribution systems; it has major limitations because of varying network conditions. In this paper, a new protective coordination technique is proposed in MV distribution networks. The proposed technique is based on calculating the rate of change of phasor voltage (*ROCOV*) in each feeder to discriminate and locate the faulty section. The measured *ROCOV* values and the required relay operating time take the shape of the standard inverse-time characteristics that are used for overcurrent relay. The system allows full coordination between the primary and backup relays. Without any need for communications, the proposed technique proved good robustness during different transient healthy conditions. The setting of the proposed relay does not need to be re-adjusted with the changes in network operating conditions since it depends on system voltage not the loading current. The proposed technique is tested using extensive MATLAB simulations under different faulty and healthy conditions in a MV distribution system. The results indicate that the proposed technique meets the fundamental protective requirements such as selectivity, reliability, sensitivity, and speed as well.

Keywords Distribution systems · Fault detection · Protection coordination · Local measurements · Rate of change of phasor voltage (*ROCOV*)

1 Introduction

Distribution systems are the largest part of the power system network, and therefore, the diagnosis of faults in these systems is a challenging task (Gabr et al. 2017). The protection system is designed to clear faults in such a way that causes the disconnection of the least possible sections of the system. Also, protective relays in distribution systems may face different kinds of problems such as fail to trip in the presence of faults or trip even though it is in healthy conditions (Abdel-Salam et al. 2017). To handle such situations, different protection schemes are presented in the literature to meet the protection system requirements. The available techniques can be classified into two main categories: non-communication protection-based schemes and communication protection-based schemes.

The overcurrent relay (OCR) is the most commonly protection type used for MV distribution networks. Inverse-time OCR is commonly used as the conventional approach for feeders in the distribution systems because of its grading time characteristic (Kiliçkiran et al. 2018). The OCR setting which is based on both the rated and fault currents is no longer valid because of varying network conditions (Shih et al. 2017). Examples for non-communication-based schemes are introduced. A time–current–voltage characteristic (TCVC) was proposed in (Saleh et al. 2015), and it relies on utilizing the fault voltage magnitude in addition to the current to calculate the operating time of modified directional OCR. The TCVC does not need any communication system and achieves reduction in total relay operating times. However, optimal settings of overcurrent relays are needed for every frequent change in network conditions. Using fault current limiters (FCLs) is

✉ Mohamed Ahmed Dawoud
en_dawoud_91@yahoo.com

[1] Electrical Power Engineering Department, Faculty of Engineering, Cairo University, Cairo, Egypt

[2] Electrical Power and Machines Department, Higher Institute of Engineering at El-Shorouk City, Cairo, Egypt

Published online: 07 February 2021

another main approach for solving the coordination problems in MV distribution systems with DGs, where several research studies are done based on finding the optimal size of FCLs (Khademi 2017; Dehghanpour et al. 2018). In fact, using FCLs will affect some relays to experience long operating times; in addition, the settings of relays or location of FCLs need to be adapted with the change in the network. Online calculation of fault currents under various system conditions by estimating the Thevenin equivalent circuit parameters is introduced in Shen et al. (2017); however, separate offline optimization technique is needed for calculating relay settings. Non-unit protection method was also investigated in Fletcher et al. (2012) for fault discrimination within DC microgrid systems. It analytically studies the current, voltage, their rate of change (*ROCOI*, *ROCOV*) and impedance profiles as measured at the generator converter terminals. For such method, there is no effective coordination method between primary and backup relays. A voltage-based protection method for distribution systems with DGs is also proposed in Jamali and Borhani-Bahabadi (2019). Such relay characteristic is formulated from extensive analysis of voltage behavior during fault conditions. The method is communication-less and independent of modes of operation. However, it is very sensitive to any slight changes in voltage, thus may lead to potential maloperation.

On the other hand, examples for communication protection-based schemes are discussed. A data-mining-based intelligent differential protection scheme is developed in Casagrande et al. (2014) and Kar et al. (2017). It relies on communicating measurements between relays at both ends of the protected feeder, where the scheme processes the faulty current and voltage signals to build a decision tree-based data mining model for registering the final relaying decision. In Jena and Samantaray (2015) and O'Brien et al. (2017), a differential protection scheme is applied with an artificial intelligent technique. The signals received from the phasor measurement units are analyzed and various features are extracted relating both operating and restraining quantities. A differential energy-based protection scheme has also been proposed in Samantaray et al. (2012), in such scheme, the fault currents at both ends of a particular feeder are retrieved and processed through modified S-transform to find out the spectral energy content for different fault situations. Adaptive protection coordination scheme of numerical DOCRs is applied in Núñez-Mata et al. (2018) under varying loading, generating conditions and components outage. In Laaksonen et al. (2014), an adaptive protection coordination scheme based on a centralized controller running the real-time analysis of the data received from the field intelligent electronic devices has been discussed. A proper communication architecture based on the LoRaWAN Class B technology was proposed for the coordination of interface protection systems in smart grids (Pasetti et al. 2020). A suitable data model structure was determined to allow the computation of the payload of the communication. In Using et al. (2014), a traveling wave-based protection scheme that uses a low bandwidth communication for meshed distribution systems with distributed generation operating as a microgrid was proposed. In Ustun and Khan (2015) and Aghdam et al. (2016), dual-setting DOCRs have been applied for meshed distribution systems with DG. Relays are coordinated in such a way to reduce the overall relay operating time for grid-connected and islanded modes. As clearly shown, the communication system plays an important role in the adaptive protection methods. However, high-cost communication infrastructure, speed, redundancy, and reliability of the communication systems are several important factors that must be considered before implementing the pervious communication-based methods (Nikolaidis et al. 2016; Hosseini et al. 2018). Moreover, communication failure may lead protection scheme to fail.

Further research studies are currently conducted toward applying the rate of change of the phasor voltage (*ROCOV*) in islanding detection and distance protection. A hybrid algorithm to identify the islanding has been proposed based on the passive parameters *ROCOV* and rate of change of reactive power (*ROCORP*) at the point of common connection of the distributed generation (DG) unit and distribution network (Rostami et al. 2017; Varma et al. 2016). Such algorithm is applied to detect DG operation modes correctly and quickly. Also, and based on *ROCOV* feature, the performance of existing conventional distance relay is improved during voltage instability conditions as proposed in Jonsson and Daalder (2002) and Sharifzadeh et al. (2014). In fact, as the impedance enters the third zone, the distance relay is blocked till the proposed algorithm accurately distinguishes the event as a fault occurrence or stressed voltage instability condition. Actually, the aforementioned methods are not designed to deal with primary and backup relays coordination to ensure secured feeders protection.

Despite the different research studies mentioned in the literature, there is a need to propose a new protection coordination approach which does not depend on the current signals that change on a wide range under different operating conditions. Therefore, the main contribution of this paper is to propose a new protection coordination technique relay suitable for MV distribution networks which is stable against all transient healthy conditions and provides a selective, reliable, and sensitive protection system in case of faults. It is based on calculating the rate of change of fundamental voltage (*ROCOV*) and relying only on local measurements. Also, it is required for the new proposed approach to avoid using communication systems

in the changing process of relay settings since it reduces system reliability and has a high cost as well.

The main contribution of this paper is as follows:

- The new protection coordination approach does not depend on the current signals as the current changes significantly with the changes occur in the MV distribution networks.
- It allows for proper coordination of primary and backup relays without a need for re-adjusting the relay setting after any changes in network operating conditions compared to the conventional protection system that needs to be upgraded. This is a result of depending on system voltage not the current.
- The proposed technique depends only upon locally available information which means it is more reliable and dependable than those that depend upon the information at the remote ends.
- The conventional voltage transformers with a low sampling frequency can be applied to implement the proposed *ROCOV* relay. It means that no additional requirements are needed over the conventional requirements of DOCRs.
- The proposed technique can well distinguish between all transient healthy and faulty conditions. Therefore, it is able to improve the performance of the protection operation considerably and thus meets the fundamental protective requirements such as reliability, sensitivity, selectivity, and speed as well.

The organization of this paper is presented as follows: methodology of the proposed technique is fully discussed in Sect. 2. Section 3 describes the test system and relays settings. Simulation results for evaluating the proposed protection relay under healthy and different faulty conditions are presented in Sects. 4 and 5, respectively. Examining the coordination capability under different faulty conditions is presented in Sect. 6. The experimental implementation of the proposed technique is introduced in Sect. 7. Evaluating the performance of the proposed technique with DG units is presented in Sect. 8. Finally, the conclusions are drawn in Sect. 9.

2 Methodology of the Proposed Technique

The voltage dip is a sudden decrease in the rated voltage magnitude which is caused by events such as starting motors or connection of heavy operating loads and faults occurring in power feeders or circuits (Omar et al. 2019).

To analyze the effect of a voltage dip due to a fault, first let us consider a three-phase solid fault as a balanced fault occurs on Line 2 at location *f* as shown in Fig. 1, where the line impedance between the relay R_2 and the fault position is xZ_{l2}. $(1-x)Z_{l2}$ is the impedance between the fault point and the load. Also, Z_{load}, Z_{l1} are the static load impedance and the impedance of Line 1 respectively.

During pre-fault condition, the measured voltage V_{pre-f} at relay R_2 can be expressed by:

$$V_{pre-f} = \frac{(Z_{l2} + Z_{load})}{Z_{l1} + Z_{l2} + Z_{load}} V_s \tag{1}$$

After the fault occurrence at point *f*, the measured voltage at relay R_2 becomes equal to V_{post-f} as given in Eq. (2):

$$V_{post-f} = \frac{[Z_f//((1-x)Z_{l2} + Z_{load})] + xZ_{l2}}{[Z_f//((1-x)Z_{l2} + Z_{load})] + xZ_{l2} + Z_{l1}} V_s \tag{2}$$

As known, the voltage dip is normally characterized in terms of the magnitude and duration. During a voltage dip, the transition from one steady state to another steady state is not immediate, but takes place with a certain speed. The temporal variation of the voltage during the transition segments is denoted here as the "rate of change of voltage". The *ROCOV* value for phase A in the proposed scheme is calculated using the following equation:

$$ROCOV = \frac{V_{A1(n)} - V_{A1(n-1)}}{\Delta T} \tag{3}$$

Here $V_{A1(n)}$ and $V_{A1(n-1)}$ are the calculated RMS values of fundamental voltage for phase A at present sample (n) and previous one $(n-1)$, respectively, while ΔT is the sampling interval.

The *ROCOV* value at relay R_2 is calculated using the pre and post RMS fault voltages by substituting Eqs. (1, 2) in Eq. 3 as follows:

$$ROCOV = \frac{V_s}{\Delta T} \times \left[\frac{(Z_{l2} + Z_{load})}{Z_{l1} + Z_{l2} + Z_{load}} - \frac{[Z_f//((1-x)Z_{l2} + Z_{load})] + xZ_{l2}}{[Z_f//((1-x)Z_{l2} + Z_{load})] + xZ_{l2} + Z_{l1}} \right] \tag{4}$$

For simplicity, assuming that: $Z_{l1} = Z_{l2} = Z$ and $Z_{load} = 20Z$, by re-arranging Eq. 4 and after some algebraic manipulations, the *ROCOV* value at relay R_2 will be given as follows:

$$ROCOV = \frac{V_s}{\Delta T} \times \frac{[(Z^3[x^2 - 42x + 441])}{(484Z^2Z_f + Z^3[-22x^2 + 440x + 462])} \tag{5}$$

As a numerical example, consider a solid three-phase fault close to the relay R_2 (at $x = 10\%$ and $Z_f = 0$), the *ROCOV* value is calculated as in Eq. 6:

$$ROCOV_{at\,10\%} = \frac{V_s}{\Delta T} \times [0.863] \tag{6}$$

Similarly, for a far solid three-phase fault from the relay R_2 (at $x = 90\%$ and $Z_f = 0$), the *ROCOV* value is calculated as in Eq. 7:

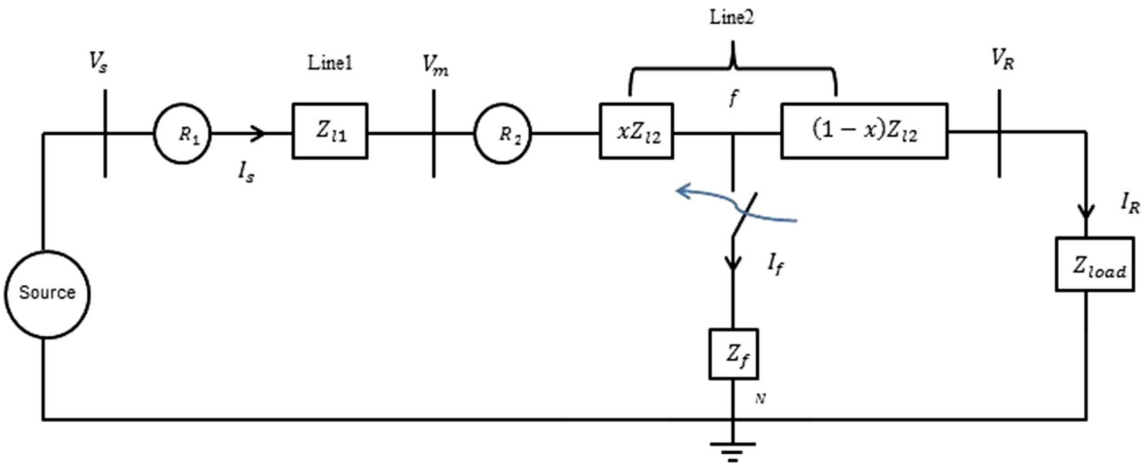

Fig. 1 Single-line diagram for a balanced fault on Line 2

$$ROCOV_{at\,90\%} = \frac{V_s}{\Delta T} \times [0.480] \tag{7}$$

As indicated in Eqs. (6, 7), the smaller the value of x in Eq. 5, the higher the value of *ROCOV*. Furthermore, the *ROCOV* values at different locations from 0 to 100% in step 10% of feeder length are estimated as shown in Fig. 2. This ensures that the closer the fault location to the relay, the higher the measured *ROCOV* value.

The proposed technique is based on the fact that the rate of change of the phasor voltage is close to zero under normal operating conditions while it jumps to higher values under fault conditions at the fault instant as shown in Fig. 3. The value of *ROCOV* is negative at the instant of fault occurrence (voltage reduction) where it has a positive value at the instant of fault clearance (voltage increase). The technique just needs only one post-fault cycle

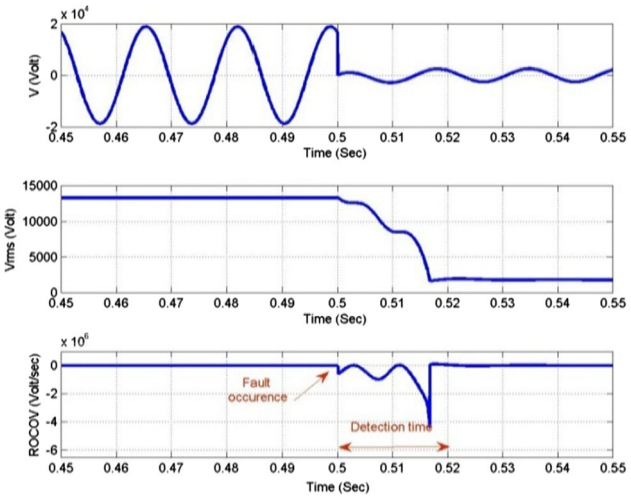

Fig. 3 Sinusoidal voltage, RMS voltage and *ROCOV* in case of a fault occurs at 0.5 s

Fig. 2 *ROCOV* changes of relay R_2 with varying the fault location in Line 2

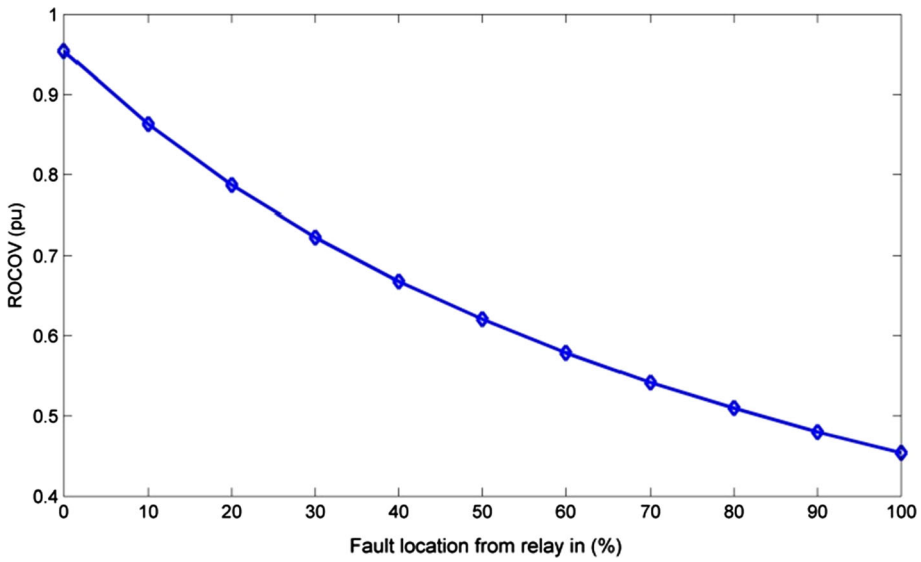

(detection time) of voltage waveform to verify the fault occurrence as the change in *ROCOV* appears only in one cycle.

Also, the simulation studies proved that the closer the fault location to the relay, the higher the values of measured *ROCOV*. Figure 4 proves the previous fact, where faults are applied on different four feeders with different current carrying capacities at different locations from 0 to 100% in step 10% of feeder length.

Moreover, Fig. 4 shows that the relation between the measured *ROCOV* values and the fault location from the relay. It takes the shape of the standard inverse-time characteristics of OCR. This feature makes the relays coordination possible using the typical inverse-time characteristics governed by Eq. (8).

$$t = TDS\left[\frac{A}{M^{\rho} - 1} + B\right] \tag{8}$$

Here:

- t is the operating time of the proposed relay.
- TDS is the time dial setting of the proposed relay.
- M is the ratio of measured *ROCOV* to $ROCOV_{pick-up}$, as $ROCOV_{pick-up}$ is the setting point value of the proposed relay.
- A, B and ρ are constants required to define the slope characteristic of the proposed relay according to IEEE Std C37.112-2018 (IEEE Power and Energy Society 2018), as illustrated in Table 1.

The relays based on the proposed technique are supposed to be installed at the beginning of each main feeder in the studied MV network. If the calculated *ROCOV* using Eq. (3) exceeds the pickup value, the relay determines the required delay time according to Eq. (8). The relay then trips at the end of the estimated delay.

A directional feature is also incorporated to discriminate between forward and reverse faults based on the sign of rate of change of current *ROCOI* forward fault has a positive value of *ROCOI* and reverse fault has a negative value. This feature is illustrated in Fig. 5. The measured *ROCOI* is calculated in a similar form to *ROCOV* Eq. (3).

As described, the proposed technique depends on the local measurements of voltage and current. In general, it is found that simple systems are more reliable. Systems depend upon local available information tend to be more reliable and dependable than those that depend upon the information at the remote end.

No additional special requirements or specifications are needed compared to the techniques depending on high frequency components (Goudarzi et al. 2015; Chaitanya and Yadav 2020). The fundamental frequency component from input phase signals are extracted using discrete Fourier transform (DFT), as presented in Wang and Dinavahi (2016). The conventional existing voltage transformers with a low sampling frequency can be applied to implement the proposed technique.

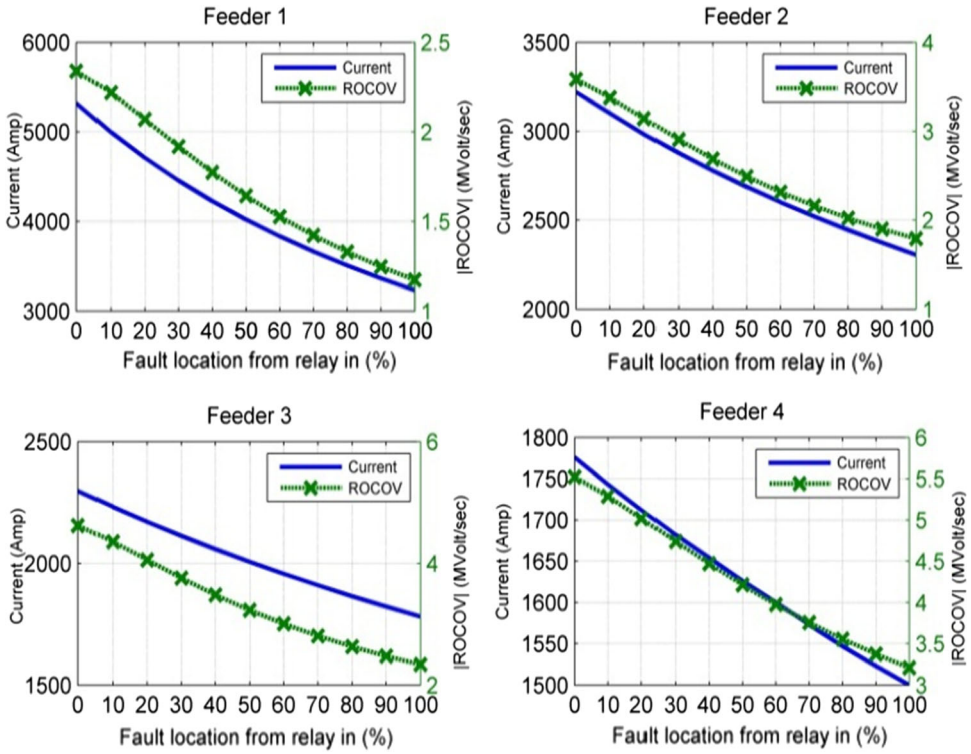

Fig. 4 Current and *ROCOV* changes with varying the fault location from relay for different feeders

Table 1 Constants for standard inverse relay characteristics

Characteristic	*A*	*B*	ρ
Moderately inverse	0.0515	0.1140	0.02
Very inverse	19.61	0.491	2
Extremely inverse	28.2	0.1217	2

3 Test System and Relays Settings

3.1 Test System Description

The proposed technique is extensively tested on the MV distribution system shown in Fig. 6, using MATLAB/Simulink. The network is a radial 22 kV with four main feeders. It is a part of the system presented in Dawoud et al. (2018). Conventional OCRs settings are calculated for the test system in order to compare OCR performance with the performance of the proposed technique. The time dial settings and pickup currents for conventional OCRs are presented in Table 2.

3.2 Setting the Proposed Relays

The proposed relay requires to know the pickup value, time dial setting, and the type of inverse characteristics in order to determine the operation time. The moderately inverse characteristic is selected for all relays with constants *A*, *B* and ρ of 0.0515, 0.114, and 0.02 respectively.

As a matter of fact, the *ROCOV* value during a fault is always higher than that during a large-load switching as shown in Fig. 7. Load switching and short-circuit studies

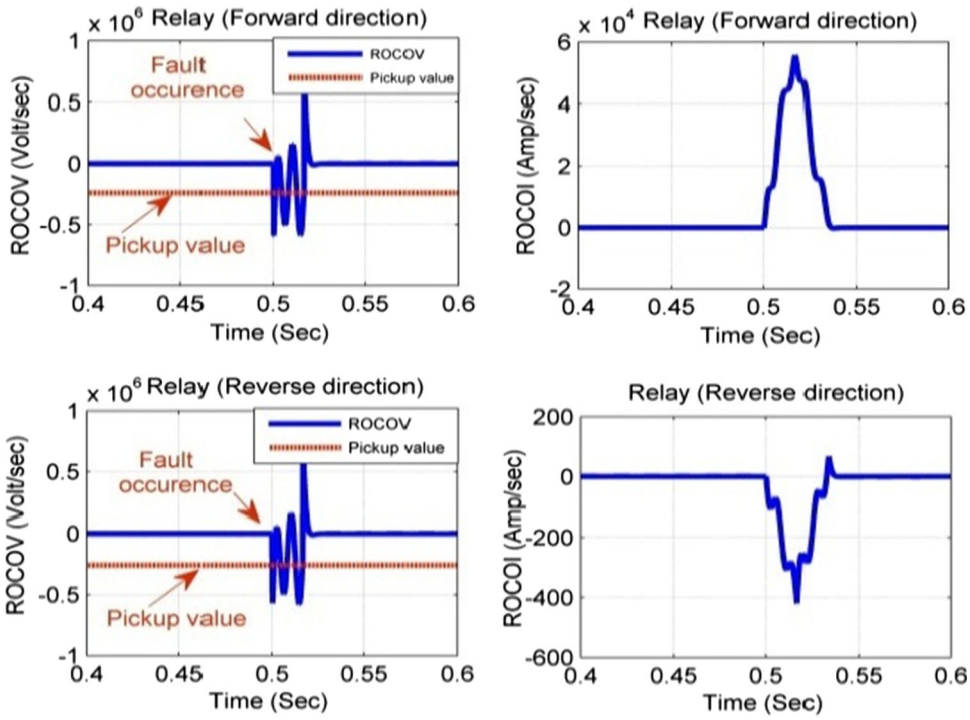

Fig. 5 *ROCOV* and *ROCOI* for two relays in forward and reverse fault direction

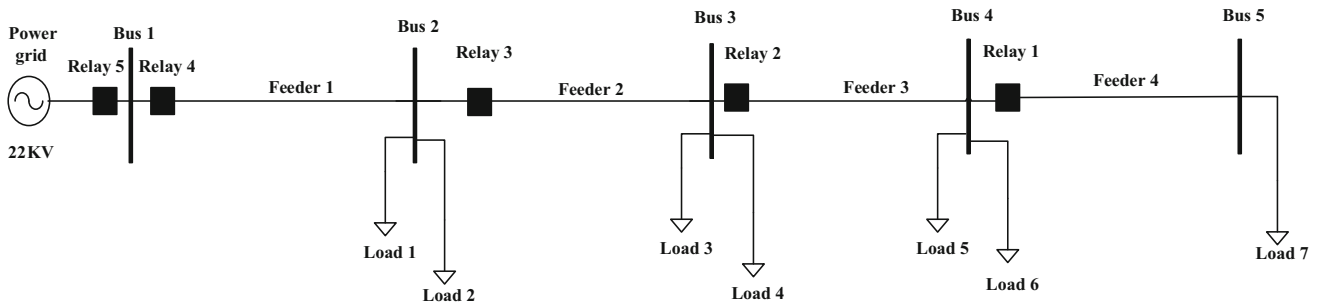

Fig. 6 Single-line diagram of 22 kV radial distribution system

Table 2 Pickup current and time dial setting for conventional OCRs

Relay no.	Pickup current (A)	*TDS* (s)
1	39.3	0.1
2	126.75	0.3694
3	221.4	0.54219
4	315	0.6672
5	315	0.8727

Table 3 Pickup and time dial settings for proposed relays

Relay no.	$\|ROCOV_{pick-up}\|$ (Volt/s)	*TDS* (s)
1	2.6×10^5	0.01
2	2.4×10^5	0.32
3	1.9×10^5	0.63
4	1.65×10^5	0.85
5	1.65×10^5	1.14

are required to determine the proper pickup value and TDS. The settings of the relays are estimated as follows:

- The $ROCOV_{pick-up}$ for each relay is chosen to be 150% of the maximum value of *ROCOV* during normal load switching case.
- To determine the proper *TDS* for all backup relays, the operating time for the relay protecting the far section is firstly chosen using Eq. 8, and then a coordination time gap of 0.3 s. is added to the backup relay time and so on.

The time dial setting and pickup value for all the relays shown in Fig. 6, are presented in Table 3. The $ROCOV_{pick-up}$ always has a negative value because the voltage is reduced at the instant of fault occurrence while it has a positive value at the instant of fault clearance. Accordingly, the trip signal is only initiated when the *ROCOV* has negative value even if the magnitude of positive *ROCOV* exceeds the absolute value of $ROCOV_{pick-up}$. To avoid false operation during transient faults, the detection time is taken as one cycle after exceeding $ROCOV_{pick-up}$ value. Rate of change of current (*ROCOI*) is estimated also to ensure that the fault is forward (positive value of *ROCOI*) as illustrated in Fig. 5.

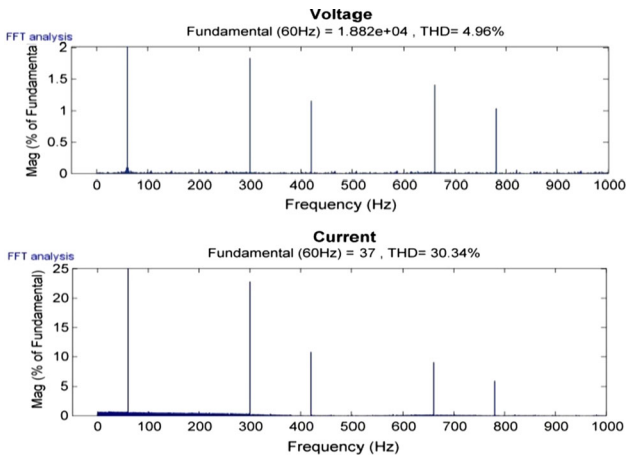

Fig. 7 Total harmonic distortion for voltage and current at PCC with nonlinear load of 0.52 MVA at bus 4

4 Testing Proposed Technique Performance Under Different Healthy Scenarios

In this section, the proposed *ROCOV* relay is tested under different transient healthy conditions such as static, dynamic load and capacitor switching to examine its stability. For all transient healthy conditions, the rate of change of voltage is less than the pickup value, and thus the protective relay does not generate any false tripping signal.

4.1 Static Load Switching Scenarios

The proposed technique was examined under complex load switching conditions According to IEEE Std 519-2014 (IEEE Power and Energy Society 2014), the harmonic voltage distortion on power networks up to 69 kV has to be limited to 5% total harmonic distortion (THD) with each individual harmonic is limited to 3%. The current harmonic limits vary depending on the maximum short-circuit current to maximum demand load current at point of common coupling (PCC). A nonlinear load is connected at bus 4 (load 6) with 0.52 MVA which produces approximately THD equals 5% and 30% in the voltage and current signals, respectively, at PCC as shown in Fig. 7. Figure 8 describes the response of the proposed relay (the load is disconnected at 0.4 s and is reconnected at 0.5 s). The value of *ROCOV* is well below the chosen pickup value, and hence, no trip signal is issued.

To verify the reliability of the proposed technique, the switching in this time is assumed to occur during unbalanced overloading condition. The load at bus 5 is simulated to operate in unbalanced manner with a 20% increase in phase-C over the normal rating as illustrated in Fig. 9. The load is then disconnected at 0.4 s and reconnected at 0.5 s. The proposed technique shows a stable performance during such complex conditions and the value of calculated *ROCOV* is lower that the pickup value as shown in Fig. 9.

4.2 Heavy Loading Scenario

Electric distribution systems are expanded, from time to time, in order to follow the changes that occur in the load

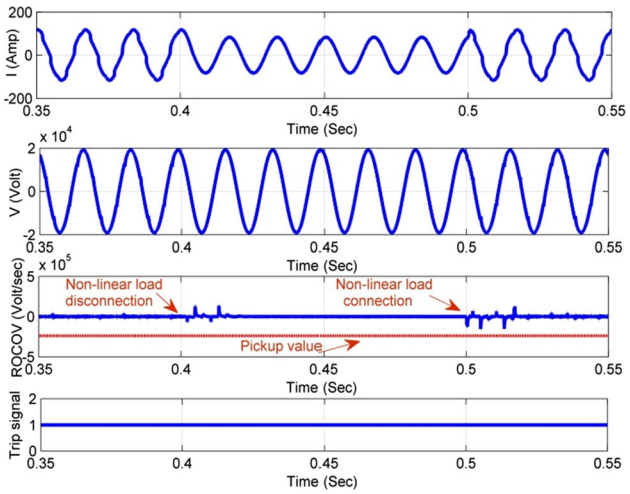

Fig. 8 Waveforms for 0.52 MVA nonlinear load switching at bus 4

(Carrano et al. 2007). The design of such networks must take into consideration not only the existing load, but also the load that is expected to exist within some time horizon. To face that increase for electrical energy demand, the conventional protection system needs to be upgraded or re-adjusted to avoid relays false tripping.

Figure 10 describes the response of the proposed relay at 0.5 s in case of adding 0.96 MVA at bus 5 which is 200% of the existing load. With conventional OCRs, the relay measured current will exceed the pickup current which is equal 39.8 amps and false operation is expected as shown in the first part of Fig. 10. On the contrary, the setting of proposed relay does not need to re-adjust as illustrated in the third part of Fig. 10.

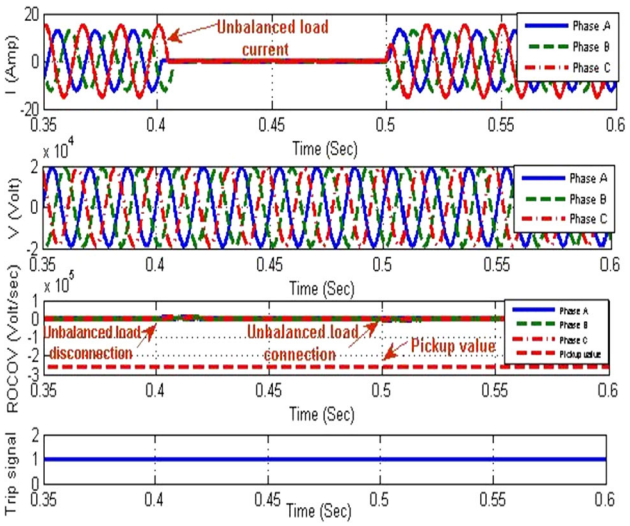

Fig. 9 Waveforms for unbalanced load switching at bus 5 (20% unbalance)

4.3 Dynamic Load Switching Scenario

At the instant of large motor switching, the electrical parameters of the power system change significantly; this may lead to false tripping of protection devices (Sreeram and Supriya 2016). Therefore, in this section, the performance of proposed relay is assessed for large motor starting condition. The static load at bus 5 is replaced by a dynamic load (induction motor) with half power rating of the static load. The test results shown in Fig. 11 ensure that the proposed relay has succeeded to distinguish between motor starting event and fault occurrence conditions. Although the starting current has exceeded the overcurrent pickup current in the time domain as in the first part of Fig. 11 (and hence the conventional OCR may face false tripping), the proposed technique was stable enough during such condition as the calculated *ROCOV* value was below the $ROCOV_{pick-up}$ as illustrated in the third and fourth part of Fig. 11.

4.4 Capacitor Disconnection Scenario

Capacitors, which are commonly connected in parallel to the power system, are commonly utilized for power factor correction, voltage sag compensation and etc. (Abou El-Ela et al. 2016). As known, at the instant of capacitor disconnection, the voltage decreases, and hence, it produces negative value of *ROCOV* as in fault case and hence the proposed technique must be tested under such conditions.

In this section, the proposed relay is evaluated for disconnecting a 350 kVAR capacitor from the end of feeder 4 (it is installed to improve the power factor from 0.78 to 0.95 lagging) as illustrated in Fig. 12. Since the value of calculated *ROCOV* is lower than the pickup value of the

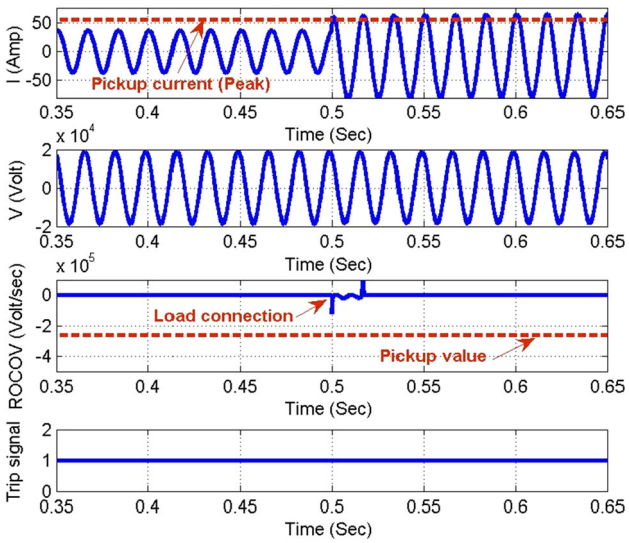

Fig. 10 Waveforms for 0.96 MVA load expansion scenario at bus 5

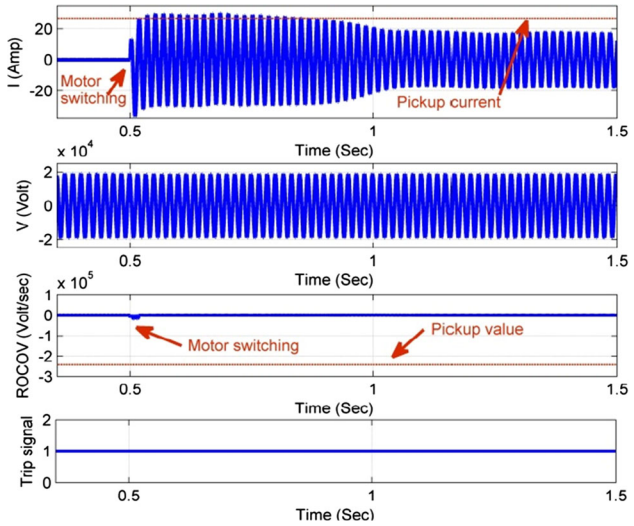

Fig. 11 Waveforms for 600 HP large motor switching scenario at the end of feeder 4

relay as illustrated in the third and fourth part of Fig. 12, the proposed technique is stable during capacitor disconnection.

The performance of the proposed technique during normal transient conditions is stable even with the existence of voltage variation because the voltage variation occurs gradually under normal conditions compared to the faulty conditions where the change in the instantaneous value of voltage is fast and large.

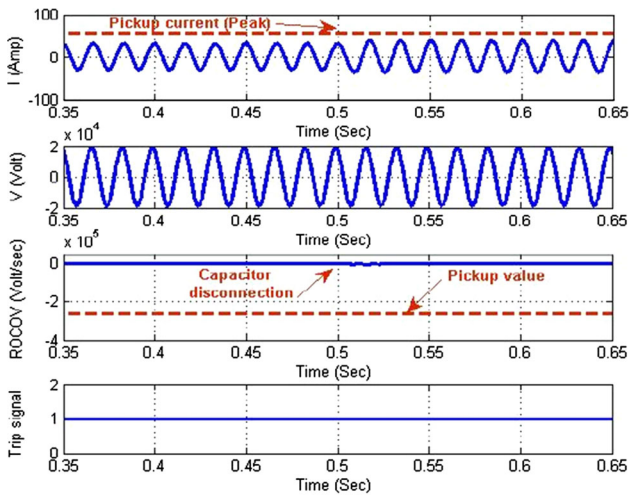

Fig. 12 Waveforms in case of 350 kVAR capacitor disconnection scenario at the end of feeder 4

5 Proposed Technique Performance under Different Fault Conditions

In this section, the proposed technique is tested under different faulty conditions to examine its reliability and sensitivity. Three-phase short-circuit fault is applied in tested cases in sections *A* and *B* as it is the most severe fault type.

5.1 Low Resistance Fault Scenario

Referring to the system shown in Fig. 6, the current and voltage signals during a typical three-phase fault at the beginning of feeder 4 are shown in Fig. 13a. The fault has occurred at 0.5 s and cleared at 0.53 s.

As shown in Fig. 13b, the value of *ROCOV* has changed from zero to a negative value higher (in magnitude) than the pickup value at the instant of fault occurrence. On other hand, the *ROCOV* value has also a positive value at the instant of fault clearing as the voltage increases.

The operating time of Relay 1 is calculated according to Eq. (8) and relay settings. The trip signal is initiated at 0.03 s after the fault occurrence as shown in Fig. 13c; the

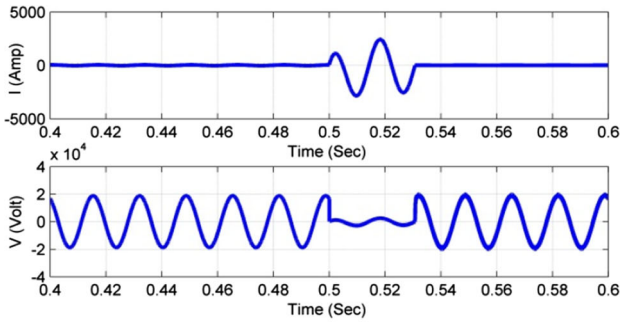

(a) Current and voltage waveforms

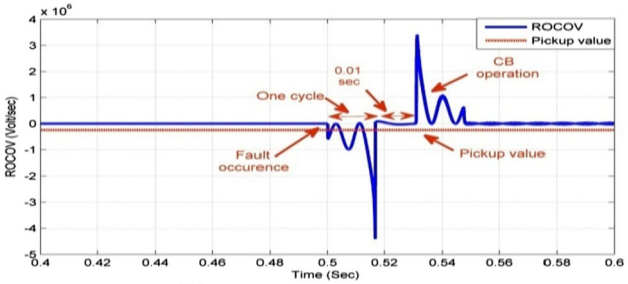

(b) Change in *ROCOV* value of Relay 1

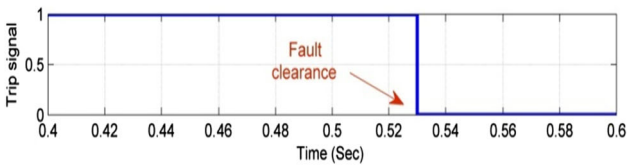

(c) Trip signal of Relay 1

Fig. 13 Three-phase fault with low resistance at the beginning of feeder 4 at 0.5 s and cleared at 0.53 s

total operating time equals 0.01 s according to Eq. (8), plus the fault detection time (0.02 s(.

5.2 High-Resistance Fault Scenario

The sensitivity of the proposed technique is examined in this section. A sensitive protection scheme must be able to detect high-resistance faults, which may have current magnitudes close to normal magnitude values, and therefore, the conventional overcurrent relays and under voltage relays may not be able to detect such faults (Mortazavi et al. 2018).

A three-phase fault is simulated at the beginning of feeder 2 with fault resistance equals 160 ohms which produces current equal 147% of the normal rated current. The conventional overcurrent relay couldn't detect such fault since the measured fault current (216.7 A) is less than the pickup current (221.4 A as presented in Table 1) as illustrated in Fig. 14a. Relay 3 with the proposed technique was able to detect such fault since the *ROCOV* value has exceeded the pickup value as shown in Fig. 14b. The results prove the sensitivity of the proposed technique.

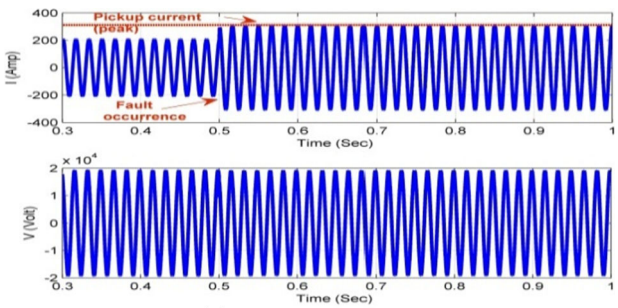

(a) Current and voltage waveforms

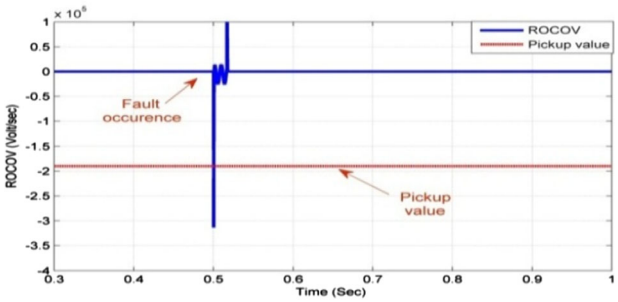

(b) Change in ***ROCOV*** value of Relay 3

Fig. 14 Three-phase fault with high resistance (160 ohms) at the beginning of feeder 2 at 0.5 s

6 Examining the Coordination Capability under Different Faulty Conditions

The main objective of this section is to examine the selectivity of the proposed *ROCOV* relay under a large variety of faulty conditions. The primary and backup relays are coordinated properly if the actual time interval between the operating times of the primary relay and the corresponding backup relay is more than the pre-specified *CTI*. To further evaluate the performance of the proposed protection relay, different case studies are simulated considering various fault types (SLG, LL, LL-G and 3L-G), location (in the four feeders), fault resistance (1, 2, 5, 6, 8, 10 and 20 Ohm), and inception angle (0°, 60°, 90° and 270°). For each fault case, the estimated *ROCOV* value and delay time for primary and backup relays are estimated as given in Table 4. The table includes five sections with a total of 20 different case studies.

The results confirmed that the proposed technique achieves the fundamental protection requirements. For example, in section (5-B in Table 4) a single line to ground fault is simulated at Feeder 3 (refer to Fig. 5) with a fault resistance of 1 ohms (other values are also examined). In this case, the value of *ROCOV* for all relays clearly exceeded the pickup value. Relay 1 will not operate because the fault is in the reverse direction since *ROCOI* has negative value. Also, it can be seen that the operating time of Relay 2 (which is the primary protection relay) equals 0.45 s, while the operating time of the first backup protection relay (Relay 3) is 0.948 s and so on for the others backup relays. The proposed technique ensures that the *CTI* is above 0.3 s.

The results show the effectiveness of the proposed technique under a large variety of faulty conditions described in the five sections in Table 4. The results also proved the selectivity feature of the proposed technique.

7 Experimental Implementation of the Proposed Technique

A simple experimental system is also designed and developed to apply the proposed technique. It includes three buses connected in radial form. The schematic figure of the experimental system with data is displayed in Fig. 15. As shown in Fig. 15, the relays are placed at the beginning of the two feeders. Load switching and short-circuit results are implemented to determine the setting of relays. The parameters of relays are illustrated in Table 5.

A general view to the whole experimental setup is illustrated in Fig. 16. Such hardware implementation is tested for different healthy and faulty cases with sampling

Table 4 Different case studies considering various fault types, fault resistance, inception angle, location and type using the proposed technique

Relay no.	(A)		(B)		(C)		(D)	
	RF = 2 Ohms		RF = 5 Ohms		RF = 10 Ohms		RF = 20 Ohms	
	$\|ROCOV\|$	t(op) (s)	$\|ROCOV\|$	t(op) (s)	$\|ROCOV\|$	t(op) (s)	$\|ROCOV\|$	t(op) (s)
Section (1): Different fault resistances (3L-G, at 20% of Feeder 4 with inception angle of 0°)								
1	2.52×10^6	0.012	1.236×10^6	0.017	7.305×10^5	0.025	5.875×10^5	0.032
2	1.407×10^6	0.494	9.071×10^5	0.648	5.833×10^5	0.956	5.206×10^5	1.092
3	8.588×10^5	1.131	5.965×10^5	1.473	4.627×10^5	1.878	4.206×10^5	2.097
4	4.515×10^5	2.249	3.396×10^5	3.107	3.133×10^5	3.488	2.833×10^5	4.075
5	4.515×10^5	3.016	3.396×10^5	4.167	3.133×10^5	4.678	2.833×10^5	5.531
Relay no.	(A)		(B)		(C)		(D)	
	$\theta = 0°$		$\theta = 60°$		$\theta = 90°$		$\theta = 270°$	
	$\|ROCOV\|$	t(op) (s)	$\|ROCOV\|$	t(op) (s)	$\|ROCOV\|$	t(op) (s)	$\|ROCOV\|$	t(op) (s)
Section (2): Different fault inception angles (3L-G, at the beginning of Feeder 3 with RF = 1 Ohm)								
1	–	–	–	–	–	–	–	–
2	3.084×10^6	0.351	3.12×10^6	0.349	4.053×10^6	0.319	4.056×10^6	0.319
3	1.277×10^6	0.907	1.28×10^6	0.906	1.609×10^6	0.815	1.608×10^6	0.8152
4	6.33×10^5	1.682	6.34×10^5	1.681	6.84×10^5	1.595	6.85×10^5	1.593
5	6.33×10^5	2.284	6.34×10^5	2.281	6.84×10^5	2.165	6.85×10^5	2.162
Relay no.	(A)		(B)		(C)		(D)	
	At Feeder 4		At Feeder 3		At Feeder 2		At Feeder 1	
	$\|ROCOV\|$	t(op) (s)	$\|ROCOV\|$	t(op) (s)	$\|ROCOV\|$	t(op) (s)	$\|ROCOV\|$	t(op) (s)
Section (3): Different fault locations (3L-G, 50% of feeder length with RF = 5 ohms, with inception angle of 270°)								
1	1.35×10^6	0.016	–	–	–	–	–	–
2	8.65×10^5	0.671	1×10^6	0.605	–	–	–	–
3	5.39×10^5	1.611	6.4×10^5	1.391	8.22×10^5	1.163	–	–
4	4.32×10^5	2.321	5.254×10^5	1.941	5.925×10^5	1.766	7.62×10^5	1.487
5	4.32×10^5	3.151	5.254×10^5	2.635	5.925×10^5	2.396	7.62×10^5	2.019
Relay no.	(A)		(B)		(C)		(D)	
	3L-G		LLG		LL		SLG	
	$\|ROCOV\|$	t(op) (s)	$\|ROCOV\|$	t(op) (s)	$\|ROCOV\|$	t(op) (s)	$\|ROCOV\|$	t(op) (s)
Section (4): Different fault types (Fault at the beginning of Feeder 4 with RF = 1 Ohm, with inception angle of 0°)								
1	4.405×10^6	0.009	3.781×10^6	0.010	1.202×10^6	0.017	1.747×10^6	0.0144
2	1.733×10^6	0.445	1.689×10^6	0.450	9.946×10^5	0.607	1.333×10^6	0.5088
3	9.7635×10^5	1.046	8.838×10^5	1.111	7.186×10^5	1.275	8.837×10^5	1.111
4	5.071×10^5	1.998	4.89×10^5	2.065	4.338×10^5	2.311	4.893×10^5	1.064
5	5.071×10^5	2.715	4.89×10^5	2.802	4.338×10^5	3.137	4.893×10^5	2.801
Relay no.	(A)		(B)		(C)		(D)	
	2L-G at Feeder 4 with RF = 5 ohms		SLG at Feeder 3 with RF = 1 ohms		3L-G at Feeder 2 with RF = 6 ohms		2L-G at Feeder 3 with RF = 8 ohms	
	$\|ROCOV\|$	t(op) (s)	$\|ROCOV\|$	t(op) (s)	$\|ROCOV\|$	t(op) (s)	$\|ROCOV\|$	t(op) (s)
Section (5): Different fault resistances, types and locations with inception angle of 0°)								
1	1.064×10^6	0.019	–	–	–	–	–	–
2	7.620×10^5	0.741	1.69×10^6	0.450	–	–	6.343×10^5	0.876

Table 4 (continued)

Relay no.	(A)		(B)		(C)		(D)	
	2L-G at Feeder 4 with RF = 5 ohms		SLG at Feeder 3 with RF = 1 ohms		3L-G at Feeder 2 with RF = 6 ohms		2L-G at Feeder 3 with RF = 8 ohms	
	$\|ROCOV\|$	t(op) (s)	$\|ROCOV\|$	t(op) (s)	$\|ROCOV\|$	t(op) (s)	$\|ROCOV\|$	t(op) (s)
3	5.059×10^5	1.712	1.17×10^6	0.948	6.07×10^5	1.452	4.804×10^5	1.804
4	2.986×10^5	3.720	6.37×10^5	1.695	4.018×10^5	2.504	3.211×10^5	3.322
5	2.986×10^5	5.049	6.37×10^5	2.273	4.018×10^5	3.398	3.211×10^5	4.509
	R1		R2		R3		R4	R5
$ROCOV_{pick-up}$	-2.6×10^5		-2.4×10		-1.9×10^5		-1.65×10^5	-1.65×10^5

The operating time t(op) of all relays is calculated using Eq. (8)

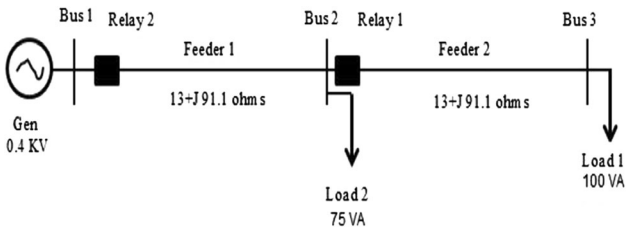

Fig. 15 Schematic diagram of the simple experimental system

frequency 1 kHz. All results of studied cases for such real hardware experimental system are extracted using digital storage oscilloscopes.

7.1 Capacitor Disconnection Scenario

In this section, the proposed relay is evaluated for 75 VAR capacitor disconnection (which produces negative value of *ROCOV* as in fault case) at the end of feeder 2 as illustrated in Fig. 17. In fact, the proposed technique was stable during capacitor disconnection since the value of calculated *ROCOV* is lower than the pickup value of the relay.

7.2 Load Connection Scenario

The proposed technique was examined under static load disconnection condition. Thus a static load (load 1) is disconnected from bus 3. Figure 18 describes the adequate response of the proposed relay in case of such case

Table 5 Pickup and time dial settings for the two relays

Relay no.	$\|ROCOV_{pick-up}\|$ (Volt/s)	*TDS* (s)
1	3×10^3	0.01
2	2.4×10^3	0.32

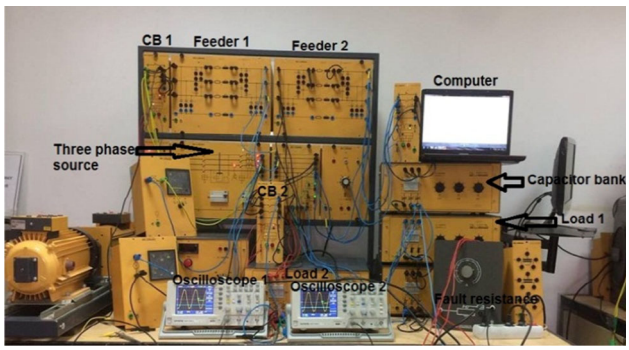

Fig. 16 General view of the hardware system setup

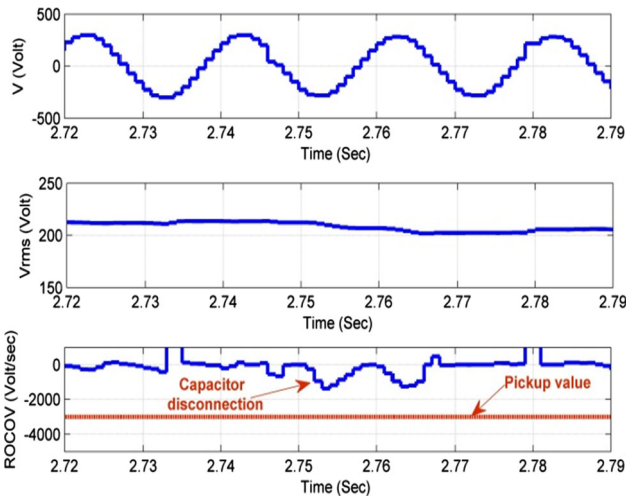

Fig. 17 Waveforms in case of 75 VAR capacitor disconnection scenario at 2.75 s

(connection occurs at 2.36 s) as the value of *ROCOV* is well below the pickup value.

7.3 Fault Scenarios

In this section, the proposed technique is tested under faulty conditions. Single-phase short-circuit fault is applied in tested cases. Figure 19 illustrates the voltage signals during a typical single-phase fault at the beginning of feeder 2 with low fault resistance 1 Ohm. The fault has occurred at 2.67 s. The value of *ROCOV* has changed to a higher (in magnitude) negative value than the pickup value at the instant of fault occurrence.

Another case is presented; a single-phase fault is applied with high fault resistance 160 ohms at the end of Feeder 2. As shown in Fig. 20, the value of *ROCOV* has changed to a negative value higher in magnitude than the pickup value at the instant of fault occurrence.

Also, the performance of the proposed protection relay is examined in this section for both primary and backup protection. Single line to ground fault is applied at the beginning of feeder 2 with different fault resistance as in Table 6. It can be deduced that the proposed technique ensures that *CTI* is above 0.3 s.

According to the previous hardware implemented tested cases, it can be ensured that the proposed technique is stable against transient healthy conditions and has high efficiency in detecting the faults.

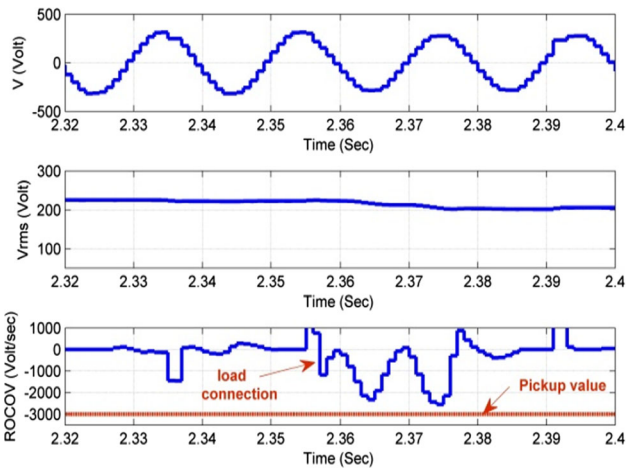

Fig. 18 Waveforms for 100 VA load connection scenario from bus 3

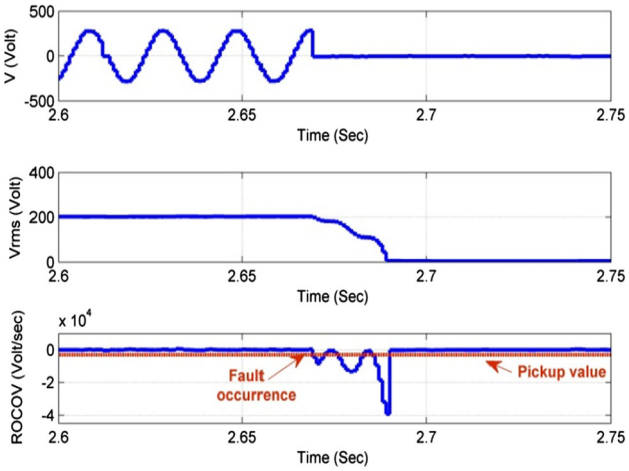

Fig. 19 Waveforms for fault occurrence with low fault resistance 1 Ohm at 2.67 s

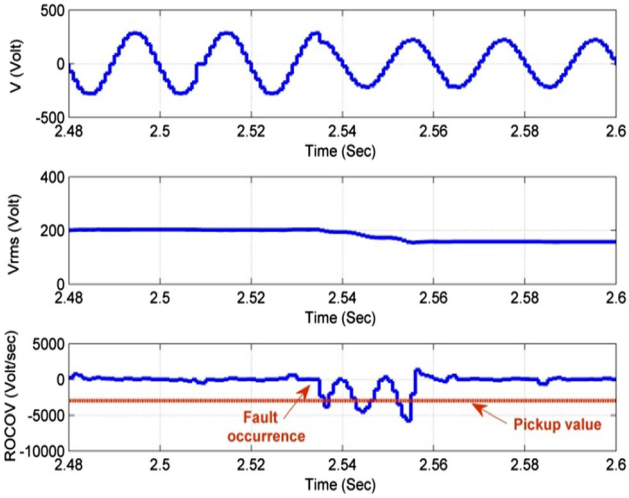

Fig. 20 Waveforms for a fault occurs at 2.53 s with high fault resistance 160 ohms

8 Evaluating the Performance of the Proposed Protection Technique with DG Units

To further verify the performance of the proposed method in presence of DG units, the IEEE 13 bus feeder is also tested with three additional inverter-based DGs as shown in Fig. 21. The inverter-based DGs of 0.1 MW are located at nodes 646, 680 and 684. The network parameters and data are presented in (Snodgrass and Xie 2020). The settings for the proposed *ROCOV* relays for such IEEE 13 bus feeder with DGs are calculated and presented in Table 7.

Tables 8 lists the relays operating time calculated using Eq. (8) in case of different fault locations based on *ROCOV*. The results in Table 8 show that the required *CTI* is maintained between all primary and backup relays pairs for all tested fault locations (F1 to F10 in Fig. 21). As

Table 6 *ROCOV* and delayed time using Eq. (8) considering various fault resistance

	Relay no. 1		Relay no. 2		*CTI* (s)
	|*ROCOV*| (Volt/s)	t(op) (s)	|*ROCOV*| (Volt/s)	t(op) (s)	
RF = 5 Ohms	3.84×10^4	0.01	6.02×10^3	0.924	0.914
RF = 10 Ohms	3.2×10^4	0.012	5.97×10^3	0.93	0.918
RF = 30 Ohms	2.2×10^4	0.014	5.9×10^3	0.95	0.936

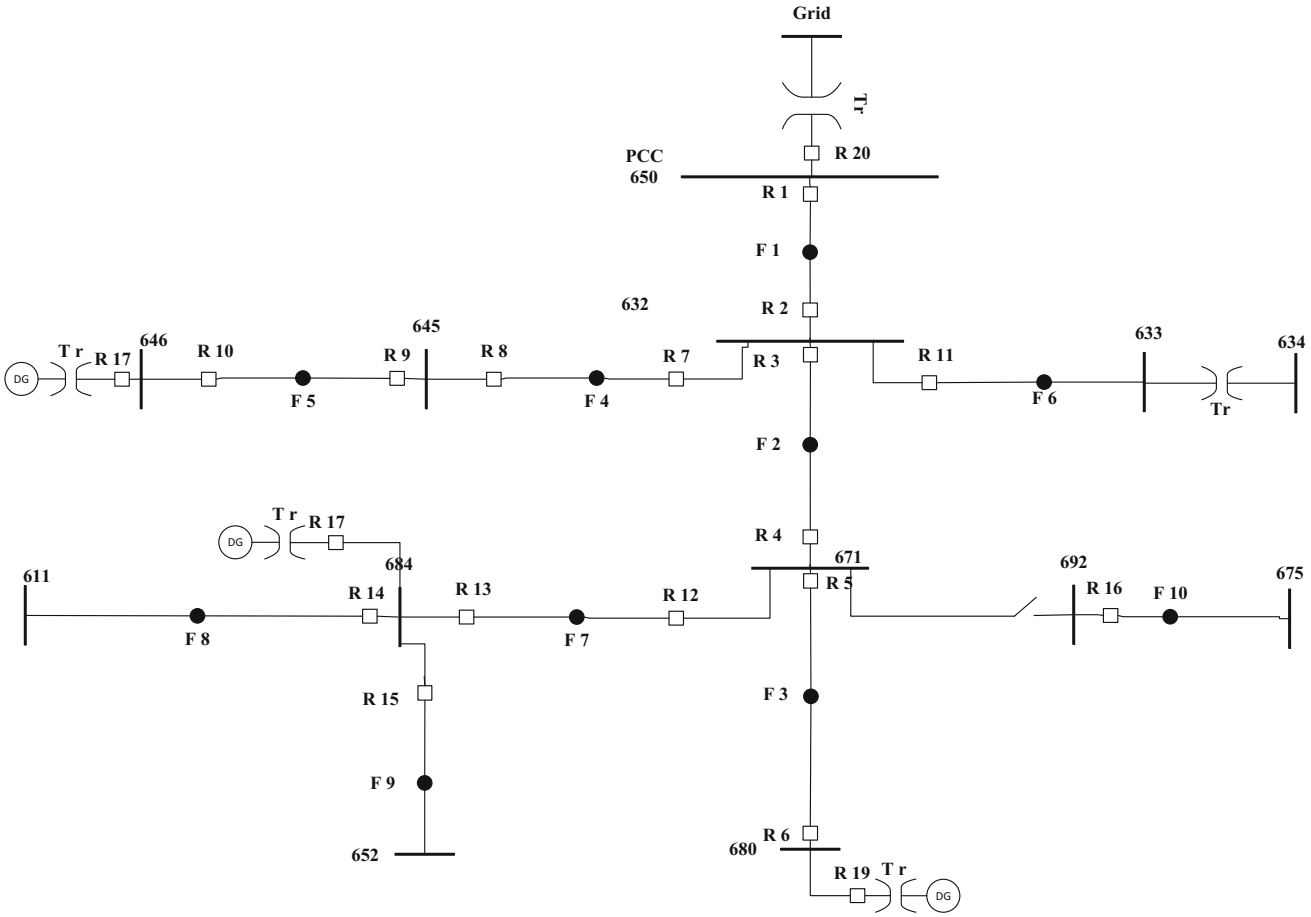

Fig. 21 IEEE 13 bus feeder embeded with DG units

shown in the table, the minimum and maximum recorded *CTI* was 0.2 and 0.5829 s respectively. The results ensure the capability to get a complete coordinated protection system using *ROCOV* relays.

As an example, for three-phase fault applied at F3, the calculated *ROCOV* value using Eq. (3) at the primary relay R5 is 8×10^5 Volt/s and at the backup relay R3 is 3×10^5 Volt/s. Based on the relays setting (*TDS* and pickup value) mentioned in Table 7, the relays operating time are calculated using Eq. (8) by 0.1648 s and 0.4682 s for primary and backup relay respectively, and thus the *CTI* is kept above 0.2.

9 Conclusion

This paper proposes a new protection coordination technique between digital relays installed in distribution networks. The proposed technique is based on estimating *ROCOV* to discriminate and locate the faulty section. The protective system with the proposed technique depends only upon locally available information which means it is more reliable and dependable than those that depends upon the information at the remote ends.

Extensive simulation results show the selectivity, sensitivity, and reliability of the proposed protection relay. The results demonstrate the stability of the relay under transient healthy conditions including dynamic load

Table 7 Settings of *ROCOV* relays in IEEE 13 bus feeder using proposed coordination technique

Relay no.	*TDS* (s)	$\lvert \boldsymbol{ROCOV}_{\boldsymbol{pick-up}} \rvert$ (Volt/s) × 10^4	Relay no.	*TDS* (s)	$\lvert \boldsymbol{ROCOV}_{\boldsymbol{pick-up}} \rvert$ (Volt/s) × 10^4
1	0.2143	1.2120	11	0.05	4.0000
2	0.05	4.0000	12	0.0921	10.1000
3	0.1368	4.0400	13	0.2716	2.4240
4	0.0961	10.1000	14	0.05	2.4000
5	0.05	10.0000	15	0.05	2.4000
6	0.1601	11.0000	16	0.05	10.0000
7	0.1151	4.0400	17	0.5552	2.0110
8	0.2796	2.0200	18	0.4059	2.4000
9	0.05	2.0000	19	0.2465	11.0385
10	0.4177	2.0080	20	0.3252	1.2047

Table 8 Operating time of *ROCOV* relays in IEEE 13 bus feeder for different fault locations

Fault location	Primary relays			Backup relays			*CTI* (s)
	Relay no.	$\lvert \boldsymbol{ROCOV} \rvert$ (Volt/s) × 10^5	t(*op*) (s)	Relay no.	$\lvert \boldsymbol{ROCOV} \rvert$ (Volt/s) × 10^5	t(*op*) (s)	
F1	R1	5	0.3885	R20	5	0.5885	0.2000
	R2	10	0.1053	R4	4	0.4821	0.3768
				R8	10	0.4823	0.3771
F2	R3	10	0.289	R1	2.38	0.4890	0.2000
				R8	9.5	0.4890	0.2000
	R4	5.5	0.3902	R6	5.5	0.6850	0.2948
				R13	5.5	0.5902	0.2000
F3	R5	8	0.1648	R3	3	0.4682	0.3034
				R13	8	0.5250	0.3602
	R6	21	0.3688	R19	21	0.5688	0.2000
F4	R7	11.8	0.2308	R1	2.5	0.4808	0.2500
				R4	4.7	0.4308	0.2000
	R8	20	0.4067	R10	20	0.6067	0.2000
F5	R9	14	0.0789	R7	6.7	0.2789	0.2000
	R10	20	0.6067	R17	20	0.8067	0.2000
F6	R11	12	0.0994	R1	2.5	0.4808	0.3814
				R4	4.65	0.4339	0.3344
				R8	11.5	0.4650	0.3656
F7	R12	12.5	0.2499	R3	3.25	0.4499	0.2000
				R6	12.5	0.4499	0.2000
	R13	21	0.4074	R18	21	0.6074	0.2000
F8	R14	21	0.0748	R12	10	0.2748	0.2000
				R18	21	0.6074	0.5326
F9	R15	14.5	0.0819	R12	8.5	0.2963	0.2144
				R18	14.5	0.6648	0.5829
F10	R16	15	0.1258	R3	3.3	0.4465	0.3208
				R6	15	0.4177	0.2919
				R13	15	0.4422	0.3164

switching and capacitor switching. The setting of proposed relay does not need to re-adjust with the changes in network operating conditions compared to the conventional protection system that needs to be upgraded to avoid false tripping. Also, the results prove full coordination between the primary and backup relays considering various fault types, location, resistance, and inception angle.

References

Abdel-Salam M, Kamel R, Sayed K, Khalaf M (2017) Design and implementation of a multifunction DSP-based-numerical relay. Electr Power Syst Res 143:32–43. https://doi.org/10.1016/j.epsr.2016.10.033

Abou El-Ela AA, Mouwafi MT, Kinawy A-M, El-Sehiemy RA (2016) Optimal capacitor placement in distribution systems for power loss reduction and voltage profile improvement. IET Gener Transm Distrib 10:1209–1221. https://doi.org/10.1049/iet-gtd.2015.0799

Aghdam TS, Karegar HK, Abbasi A (2016) Discussion on "Optimal Protection Coordination for Meshed Distribution Systems with DG Using Dual Setting Relays". IEEE Trans Smart Grid 7:1756. https://doi.org/10.1109/TSG.2016.2548878

Carrano EG, Guimarães FG, Takahashi RHC, Neto OM, Campelo F (2007) Electric distribution network expansion under load-evolution uncertainty using an immun system inspired algorithm. IEEE Trans Power Syst 22:851–861. https://doi.org/10.1109/TPWRS.2007.894847

Casagrande E, Woon WL, Zeineldin HH, Svetinovic D (2014) Scheme for microgrids with inverter-based distributed generators. IEEE Trans Smart Grid 5:29–37

Chaitanya BK, Yadav A (2020) An intelligent faulty line identification scheme for micro-grids. Iran J Sci Technol Trans Electr Eng 44:537–549. https://doi.org/10.1007/s40998-019-00247-x

Dawoud MA, Ibrahim DK, Gilany M (2018) Restoring recloser-fuse coordination in radial distribution networks with distributed generation. In: 2017 19th International middle-east power systems conference, MEPCON 2017 Proceedings

Dehghanpour E, Kazemi Karegar H, Kheirollahi R, Soleymani T (2018) Optimal coordination of directional overcurrent relays in microgrids by using cuckoo-linear optimization algorithm and fault current limiter. IEEE Trans Smart Grid 9:1365–1375. https://doi.org/10.1109/TSG.2016.2587725

Fletcher SDA, Norman PJ, Galloway SJ, Burt GM (2012) Analysis of the effectiveness of non-unit protection methods within DC microgrids. 111–111. https://doi.org/10.1049/cp.2011.0142

Gabr MA, Ibrahim DK, Ahmed ES, Gilany MI (2017) A new impedance-based fault location scheme for overhead unbalanced radial distribution networks. Electr Power Syst Res 142:153–162. https://doi.org/10.1016/j.epsr.2016.09.015

Goudarzi M, Vahidi B, Naghizadeh RA, Hosseinian SH (2015) Improved fault location algorithm for radial distribution systems with discrete and continuous wavelet analysis. Int J Electr Power Energy Syst 67:423–430. https://doi.org/10.1016/j.ijepes.2014.12.014

Hosseini SA, Askarian Abyaneh H, Sadeghi SHH, Eslami R (2018) Improving adaptive protection to reduce sensitivity to uncertainties which affect protection coordination of microgrids. Iran J Sci Technol Trans Electr Eng 42:63–74. https://doi.org/10.1007/s40998-018-0049-5

IEEE Power and Energy Society (2014) IEEE recommended practice and requirements for harmonic control in electric power systems IEEE Power and Energy Society. ANSI/IEEE Std 519(2014):5–9. https://doi.org/10.1109/IEEESTD.2014.6826459

IEEE Power and Energy Society (2018) IEEE Standard for Inverse-Time Characteristics Equations for Overcurrent Relays IEEE Standard for Inverse- Time Characteristics Equations for Overcurrent Relays

Jamali S, Borhani-Bahabadi H (2019) Protection method for radial distribution systems with DG using local voltage measurements. IEEE Trans Power Deliv 34:651–660. https://doi.org/10.1109/TPWRD.2018.2889895

Jena MK, Samantaray SR (2015) Synchrophasors-assisted IPII-based intelligent relaying for transmission lines including UPFC. Int J Emerg Electr Power Syst 16:1–10. https://doi.org/10.1515/ijeeps-2014-0134

Jonsson M, Daalder J (2002) An adaptive scheme to prevent undesirable distance protection operation during voltage instability. IEEE Power Eng Rev 22:61. https://doi.org/10.1109/MPER.2002.4311847

Kar S, Samantaray SR, Zadeh MD (2017) Data-mining model based intelligent differential microgrid protection scheme. IEEE Syst J 11:1161–1169. https://doi.org/10.1109/JSYST.2014.2380432

Khademi MM (2017) Paper 0192 designing a coordinated protection system for microgrids enabled. Cired 2017:12–15

Kiliçkiran HC, Şengör İ, Akdemir H, Kekezoğlu B, Erdinç O, Paterakis NG (2018) Power system protection with digital overcurrent relays: a review of non-standard characteristics. Electr Power Syst Res 164:89–102. https://doi.org/10.1016/j.epsr.2018.07.008

Laaksonen H, Ishchenko D, Oudalov A (2014) Adaptive protection and microgrid control design for Hailuoto Island. IEEE Trans Smart Grid 5:1486–1493. https://doi.org/10.1109/TSG.2013.2287672

Mortazavi SH, Moravej Z, Shahrtash SM (2018) A hybrid method for arcing faults detection in large distribution networks. Int J Electr Power Energy Syst 94:141–150. https://doi.org/10.1016/j.ijepes.2017.06.036

Nikolaidis VC, Papanikolaou E, Safigianni AS (2016) A communication-assisted overcurrent protection scheme for radial distribution systems with distributed generation. IEEE Trans Smart Grid 7:114–123. https://doi.org/10.1109/TSG.2015.2411216

Núñez-Mata O, Palma-Behnke R, Valencia F, Mendoza-Araya P, Jiménez-Estévez G (2018) Adaptive protection system for microgrids based on a robust optimization strategy. Energies. https://doi.org/10.3390/en11020308

O'Brien W, Udren E, Garg K, Haes D, Sridharan B (2017) Catching falling conductors in midair—detecting and tripping broken distribution circuit conductors at protection speeds. 69th Annu Conf Prot Relay Eng CPRE 2016. https://doi.org/10.1109/CPRE.2016.7914881

Omar AI, Abdel Aleem SHE, El-Zahab EEA, Algablawy M, Ali ZM (2019) An improved approach for robust control of dynamic voltage restorer and power quality enhancement using grasshopper optimization algorithm. ISA Trans. https://doi.org/10.1016/j.isatra.2019.05.001

Pasetti M, Sisinni E, Ferrari P, Rinaldi S, Depari A, Bellagente P, Della Giustina D, Flammini A (2020) Evaluation of the use of class B LoraWAn for the coordination of distributed interface protection systems in smart grids. J Sens Actuator Netw 9:1–22. https://doi.org/10.3390/jsan9010013

Rostami A, Abdi H, Moradi M, Olamaei J, Naderi E (2017) Islanding detection based on ROCOV and ROCORP parameters in the presence of synchronous DG applying the capacitor connection strategy. Electr Power Compon Syst 45:315–330. https://doi.org/10.1080/15325008.2016.1250842

Saleh KA, Zeineldin HH, Al-Hinai A, El-Saadany EF (2015) Optimal coordination of directional overcurrent relays using a new time-current-voltage characteristic. IEEE Trans Power Deliv 30:537–544. https://doi.org/10.1109/TPWRD.2014.2341666

Samantaray SR, Joos G, Kamwa I (2012) Differential energy based microgrid protection against fault conditions. IEEE PES Innov Smart Grid Technol ISGT 2012:1–7. https://doi.org/10.1109/ISGT.2012.6175532

Sharifzadeh M, Lesani H, Sanaye-Pasand M (2014) A new algorithm to stabilize distance relay operation during voltage-degraded conditions. IEEE Trans Power Deliv 29:1639–1647. https://doi.org/10.1109/TPWRD.2013.2285502

Shen S, Lin D, Wang H, Hu P, Jiang K, Lin D, He B (2017) An adaptive protection scheme for distribution systems with DGs based on optimized thevenin equivalent parameters estimation. IEEE Trans Power Deliv 32:411–419. https://doi.org/10.1109/TPWRD.2015.2506155

Shih MY, Conde A, Leonowicz Z, Martirano L (2017) An adaptive overcurrent coordination scheme to improve relay sensitivity and overcome drawbacks due to distributed generation in smart grids. IEEE Trans Ind Appl 53:5217–5228. https://doi.org/10.1109/TIA.2017.2717880

Snodgrass J, Xie L (2020) Overvoltage analysis and protection of lightning arresters in distribution systems with distributed generation. Int J Electr Power Energy Syst 123:106209. https://doi.org/10.1016/j.ijepes.2020.106209

Sreeram V, Supriya MV (2016) Fault current discrimination during induction motor starting. 2016 IEEE 6th Int Conf Power Syst ICPS 2016 6–9. https://doi.org/10.1109/ICPES.2016.7584168

Using IM, Li X, Member S, Dy A, Burt GM (2014) Traveling wave-based protection scheme for mathematical morphology. IEEE Trans Smart Grid 5:2211–2218. https://doi.org/10.1109/TSG.2014.2320365

Ustun TS, Khan RH (2015) Multiterminal hybrid protection of microgrids over wireless communications network. IEEE Trans Smart Grid 6:2493–2500. https://doi.org/10.1109/TSG.2015.2406886

Varma RK, Rahman SA, Atodaria V, Mohan S, Vanderheide T (2016) Technique for fast detection of short circuit current in PV distributed generator. IEEE Power Energy Technol Syst J 3:155–165. https://doi.org/10.1109/jpets.2016.2592465

Wang Y, Dinavahi V (2016) Real-time digital multi-function protection system on reconfigurable hardware. IET Gener Transm Distrib 10:2295–2305. https://doi.org/10.1049/iet-gtd.2015.0718